JOURNAL OF COMPUTATIONAL PHYSICS 11, 591–605 (1973)

# Stability Analysis of Low-Pressure Axisymmetric Toroidal Plasma Simulations

RAY C. GRIMM

*UKAEA Culham Laboratory, Abingdon, Berkshire*

AND

JOHN L. JOHNSON*

*Princeton University Plasma Physics Laboratory, Princeton, N. J. 08540*

Received May 19, 1972

A study of the local stability of a numerical algorithm for simulating two-dimensional small inverse-aspect-ratio plasma confinement leads to an amplification matrix closely related to the dispersion relation given by an analytic treatment. Both leapfrog and Lax–Wendroff schemes are carried through; the latter provides results in good agreement with the physics.

## 1. INTRODUCTION

The magnetohydrodynamical description of low-$\beta$ axisymmetric toroidal plasma devices has received considerable attention in recent years [1–9]. Simultaneously, much effort has been expended in constructing computer simulation models [10–13]. With these one can determine the time evolution of nonstationary states and thereby study the properties of equilibrium configurations, such as the rate of steady state diffusion and the flows of heat and mass in the system. This possibility of following the nonlinear development of unstable modes greatly compliments the analytical work and provides understanding of the physical processes involved.

A numerical procedure for following the time development of a system from its initial configuration was presented previously [10]. Careful consideration was given to the satisfaction of certain constraints exhibited by the physical system; for example, the equations were solved in a manner that ensures conservation of charge neutrality and every effort was made to prevent the introduction of enhanced

* On loan from Westinghouse Research Laboratories.

numerical transport across the field lines. The explicit finite difference schemes for the individual equations were chosen separately with regard to attaining sufficient accuracy for the measurement of growth rates and for the detailed spatial resolution necessary for studying the physical processes involved. Long term application has demonstrated that the techniques involve no disastrous numerical instabilities, although the presence of numerical viscosity has demanded the adoption of different schemes in at least one application [12].

The choice of different finite difference schemes for the separate equations, however, makes numerical analysis of the simulation as a whole virtually impossible; however, the numerical stability of the various modes of oscillation present was demonstrated individually [10]. On the other hand in most of the applications to which the code has been applied it is just this interaction between the various modes which provides the interesting physical phenomena, and one would like to be assured that the numerical simulation is providing an accurate and convergent representation of these effects. Here we suggest similar finite difference schemes for the representation of the various differential operators in each of the appropriate equations, and demonstrate the consistency and numerical stability of this simulation.

In the next section we present the physical model, and the manner in which the simulation is to be attempted. In Section 3 we simplify this set of nonlinear equations to a form from which the well-known numerical analysis results can be applied. The leapfrog scheme is discussed in Section 4, while Section 5 is devoted to the simple two-step Lax–Wendroff scheme. Some simple results are given to illustrate the stability arguments.

## 2. Model and Simulation Method

We describe the time evolution of the following set of simple hydromagnetic equations, appropriate to a toroidal low-$\beta$ plasma device [6]:

$$\rho \frac{d\mathbf{v}}{dt} = \frac{1}{c}\mathbf{J} \times \mathbf{B} - v_{th}^2 \nabla\rho, \tag{1}$$

$$\nabla\phi = \frac{1}{c}\mathbf{v} \times \mathbf{B} - \eta\mathbf{J}, \tag{2}$$

$$\frac{\partial\rho}{\partial t} + \nabla \cdot \rho\mathbf{v} = 0, \tag{3}$$

and

$$\nabla \cdot \mathbf{J} = 0. \tag{4}$$

Here $v_{th} \equiv (2kT/M)^{1/2}$ is the thermal speed. We adopt the usual axisymmetric model with magnetic field given by

$$\mathbf{B} = (B_0/N)(f(r)\,\mathbf{e}_\theta + \mathbf{e}_z), \tag{5}$$

where

$$N \equiv 1 - \epsilon \cos\theta, \qquad \epsilon \equiv r/R.$$

The geometry is illustrated in Figure 1. We decompose vectors into directions parallel to the magnetic field, perpendicular to the magnetic surfaces, and normal to both of these; then

$$\mathbf{v} = v_r\mathbf{e}_r + v_s B_0(\mathbf{B} \times \mathbf{e}_r)/B^2 + v_b B_0(\mathbf{B}/B^2). \tag{6}$$

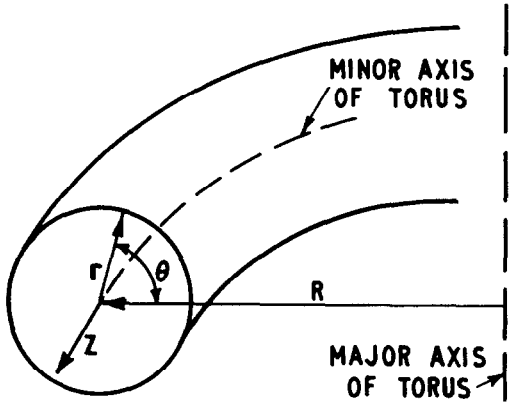


FIG. 1. The toroidal coordinate system.

Equations (1) through (4) describe a coupled closed system which is solved to advance $\rho$, $\mathbf{v}$, $\mathbf{J}$ and $\phi$ in time, given their initial configurations.

The method for solving these equations has been presented previously [10]; for completeness we briefly summarise it again here.

The component of Eq. (1) parallel to $\mathbf{B}$ is used to advance $v_b$ forward in time. Since the right-hand side of this equation in the perpendicular directions is small near equilibrium situations, we use these components to determine $\mathbf{J}_\perp$. Knowing $\mathbf{J}_\perp$ we evaluate the part of $J_b/B$ that varies along a field line by means of Eq. (4). We then use the parallel component of Eq. (2) to obtain the part of the electrostatic potential $\hat{\phi}$ which varies on a magnetic surface. The constant of integration in $J_b/B$ is determined from the condition that $\hat{\phi}$ be single valued. The surface constant $\langle\phi\rangle$ is advanced in time using the '$r$' component of Eq. (2), the

'$s$' component of Eq. (1) and the charge conservation constraint (which is necessary for $J_b$ to be single valued)

$$\oint d\theta\, NJ_r = 0. \tag{7}$$

Once the total potential $\phi = \langle\phi(r)\rangle + \hat{\phi}(r, \theta)$ has been evaluated at the new time, the perpendicular components of Ohm's law are used to update $\mathbf{v}_\perp$. Finally, $\rho$ is found at the new time from Eq. (3). Although it is not possible to completely time and space center each of the terms in the system of equations (the inertial terms are particularly difficult), second order accuracy can be approached by iterating. The scheme can be implemented in such a manner, however, that terms that are not correctly time-centered are small, and in fact experience has shown that in many cases iteration is not necessary.

We have implemented this procedure by constructing an area-conserving grid with points equally spaced in $\Psi$ and $\Phi$, where $\Psi$ represents a magnetic flux and $\Phi$ is analogous to a magnetic scalar potential. Thus, the program is applicable to realistic axisymmetric configurations, such as tokamaks and levitrons, where the magnetic surfaces need not be concentric or even circular. For the purpose of this discussion we use $r^2$ and $\theta$ for our grid, as shown in Fig. 2, so that our magnetic surfaces are concentric circles. We define the plasma quantities on each of these grid points at some particular time as indicated in the figure legend and introduce a straightforward finite-difference scheme (leapfrog or Lax–Wendroff) to advance

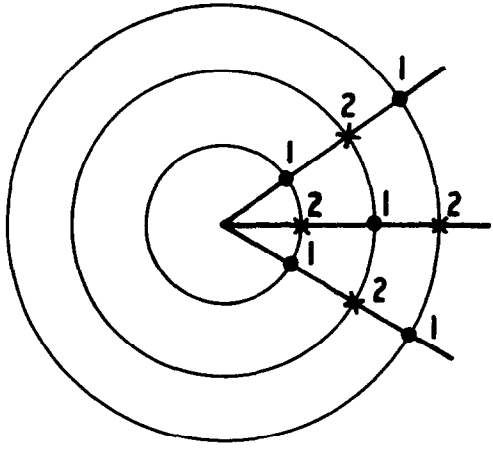


FIG. 2. The two-step finite-difference grid. For the Lax–Wendroff scheme, grid (1) contains the values of $\rho$, $\mathbf{v}$ at even time steps and intermediate values of $\mathbf{J}, \phi$ at odd time steps, while grid (2) contains intermediate values of $\rho$, $\mathbf{v}$ appropriate to odd time steps and values of $\mathbf{J}, \phi$ at even time steps. For the leapfrog scheme both grids have equal weight.

them in time. In addition to geometry this scheme differs from the previous ones [10, 12] in that the three parameters $\rho$, $v_b$, and $\langle\phi\rangle$ are advanced in time with the same scheme rather than with different ones. To effect this requires staggering the quantities on the mesh somewhat differently from what was done before. An iteration scheme is also incorporated to update the perpendicular velocity so as to keep second-order accuracy in the time advancement. Finally, in the application of the Lax–Wendroff scheme we average over only the two neighboring points on the magnetic surface rather than the four neighboring points. This eliminates undesirable coupling of the surfaces so that the physics is better represented by the model. The program has been implemented in a Symbolic Algol form [14] as well as in a Fortran version [15].

## 3. The Simplified Finite-Difference Equations

In order to discuss the consistency and stability of the finite-difference representations of Eqs. (1) to (4), we make several reasonable approximations.

For the first part, we restrict consideration to checking the "local" stability of the linearized equations by taking, for example,

$$\rho_{ij}^n = \rho_{ij}^n + \tilde{\rho}_{ij}^n \tag{8}$$

(upper indices refer to the time step, lower to grid locations $1 \leqslant i \leqslant N_r$, $0 \leqslant j \leqslant N_\theta$). Here the perturbations $\tilde{\rho}_{ij}^n$ are assumed to be small compared to the "steady state" part of the solution $\rho_{ij}^n$. Similar linearizations hold for the other time-dependent variables.

A second important simplification arises from the observation that in most physical situations there are two distinct physical time scales [6]: the time for the resistive diffusion of the plasma across the magnetic surfaces and that for the propagation of acoustic disturbances along the field lines. The former provides the major coupling of the various surfaces and occurs on a time scale very much longer than that of acoustic wave phenomena. To effect this simplification we adopt a small inverse-aspect-ratio expansion and assume

$$\epsilon \equiv \frac{r}{R} \sim f \sim \frac{\eta}{f^2} \sim \frac{v_s}{v_{th}} \sim \frac{f v_b}{v_{th}} \ll 1,$$

so that, in particular, $v_r \sim 0(\epsilon^2)$. Since in all the equations affecting the stability analysis derivatives with respect to $r$ occur only multiplied by $v_r$, this expansion reduces the stability problem to a one-dimensional situation. Henceforth, the finite difference equations refer only to a particular magnetic surface; we therefore drop the '$r$' index. We also assume that $v_b^{(0)} = 0$ on the surface of interest. This makes $v_s^{(1)} = v_\theta^{(1)}$, the lowest-order poloidal velocity.

These approximations reduce the problem of determining the stability of the numerical scheme to a set of finite-difference equations that advance in time $\tilde{u} \equiv [\partial\langle\tilde{\phi}\rangle/\partial r] = \sum_j (\tilde{v}_{s,j}/N_j)$ which represents the '$s$' component of the velocity perturbation, $\tilde{v}_j$ the '$b$' component, and $\tilde{\rho}_j$ the density perturbation, at each point $j$ on the pertinent grid. We introduce the parameters

$$\sigma = 0, \quad \kappa = 1 \quad \text{for Lax–Wendroff two-step scheme,}$$
$$\sigma = 1, \quad \kappa = 2 \quad \text{for leapfrog scheme,}$$

so that the same code applies to either numerical scheme. We use the usual centered-difference operator $\delta$ and averaging operator $\mu$ such that, when operating on a function $x$,

$$\delta x_j^n \equiv x_{j+1}^n - x_{j-1}^n ,$$
$$\mu x_j^n \equiv \tfrac{1}{2}(x_{j+1}^n + x_{j-1}^n).$$

In the analysis these operators act on some equilibrium quantities as well as the perturbations. Thus, on one grid

$$\tilde{u}^{2n+1} = \tilde{u}^{2n-1} + 2\Delta t \sum Q_{12,2j}\tilde{\rho}_{2j}^{2n}, \tag{9}$$

$$\tilde{\rho}_{2j+1}^{2n+1} = \tilde{\rho}_{2j+1}^{2n-1} + 2\Delta t(Q_{21,2j+1}\tilde{u}^{2n} + Q_{22}\,\delta\tilde{\rho}_{2j+1}^{2n} + Q_{23}\,\delta\tilde{v}_{2j+1}^{2n}, \tag{10}$$

$$\tilde{v}_{2j+1}^{2n+1} = \tilde{v}_{2j+1}^{2n-1} + 2\Delta t(Q_{31,2j+1}\tilde{u}^{2n} + Q_{32}\,\delta\tilde{\rho}_{2j+1}^{2n} + Q_{33}\,\delta\tilde{v}_{2j+1}^{2n}); \tag{11}$$

the two-step procedure is completed by filling in the alternative grid according to

$$\tilde{u}^{2n} = \sigma\tilde{u}^{2n-2} + (1-\sigma)\,\tilde{u}^{2n-1} + \kappa\,\Delta t \sum Q_{12,2j+1}\tilde{\rho}_{2j+1}^{2n-1}, \tag{12}$$

$$\tilde{\rho}_{2j}^{2n} = \sigma\tilde{\rho}_{2j}^{2n-2} + (1-\sigma)\,\mu\tilde{\rho}_{2j}^{2n-1} + \kappa\,\Delta t(Q_{21,2j}\tilde{u}^{2n-1} + Q_{22}\,\delta\tilde{\rho}_{2j}^{2n-1} + Q_{23}\,\delta\tilde{v}_{2j}^{2n-1}), \tag{13}$$

and

$$\tilde{v}_{2j}^{2n} = \sigma\tilde{v}_{2j}^{2n-2} + (1-\sigma)\,\mu\tilde{v}_{2j}^{2n-1} + \kappa\,\Delta t(Q_{31,2j}\tilde{u}^{2n-1} + Q_{32}\,\delta\tilde{\rho}_{2j}^{2n-1} + Q_{33}\,\delta\tilde{v}_{2j}^{2n-1}). \tag{14}$$

The non-zero elements of the matrix $Q$ are

$$Q_{12,j} = -v_{th}^2(\delta\cos\theta_j)/\rho^{(0)}R\,\Delta\theta,$$
$$Q_{21,j} = -[(\delta\rho_j^{(1)}) - 2r\rho^{(0)}(\delta\cos\theta_j)/R]/2r\,\Delta\theta,$$
$$Q_{22} = -v_\theta^{(1)}/2r\,\Delta\theta,$$
$$Q_{23} = -f\rho^{(0)}/2r\,\Delta\theta,$$
$$Q_{31,j} = -(\delta v_{bj}^{(1)})/2r\,\Delta\theta,$$
$$Q_{32} = -fv_{th}^2/2\rho^{(0)}r\,\Delta\theta,$$
$$Q_{33} = v_\theta^{(1)}/2r\,\Delta\theta.$$

Here we have adopted the notation employed in the analytic work [6] of carrying bracketed superscripts to indicate the appropriate order in the inverse-aspect-ratio expansion.

The stability analysis proceeds in the usual way [16]. We expand all quantities in Fourier series. This is especially useful for this model because the $\epsilon$ expansion makes the equilibrium expressible in terms of simple trigonometric functions. Thus,

$$\rho_j = \rho^{(0)} + \rho_s^{(1)} \sin\theta_j + \rho_c^{(1)} \cos\theta_j + \cdots, \tag{15}$$

with similar expressions for the other equilibrium functions. These coefficients are given in reference 6. Likewise,

$$\tilde{v}_j{}^n = \tilde{v}_0{}^n + \sum_{k=1}^{\infty} (\tilde{v}_{sk}^n \sin(k\theta_j) + \tilde{v}_{ck}^n \cos(k\theta_j)). \tag{16}$$

Then, substituting these into the finite difference equations and using the orthogonality properties of the trigonometric functions, we obtain a set of algebraic equations relating the Fourier modes of the perturbed quantities at different times. Defining the amplification factor for each mode

$$\lambda(k) \equiv \tilde{v}_{sk}^{2n+2}/\tilde{v}_{sk}^{2n},$$

we obtain the amplification matrix (**A**) for the finite-difference scheme. Stability in the usual sense (Neumann's sufficient condition [16]) requires that the spectral radius of **A** satisfy $\rho(\mathbf{A}) \leqslant 1 + O(\Delta t)$. Alternatively, by demanding that the system of algebraic equations obtained has a non-trivial solution, we recover the finite difference analogue of the analytical dispersion relation. The two approaches are equivalent of course, but it is physically instructive to pursue the latter course.

## 4. The Leapfrog Scheme

Here each step in the procedure has equal weight, so that the main and auxiliary grids contain approximations to the solution at even and odd timesteps. We write the amplification factor for each step as $\xi(k)$, so that

$$\tilde{v}_{sk}^{2n+2} = \xi(k)\, \tilde{v}_{sk}^{2n+1} = \xi^2(k)\, \tilde{v}_{sk}^{2n}.$$

Now straightforward application of the steps described above leads to the set of coupled equations

$$\mathbf{D}\cdot\mathbf{x} \equiv \begin{bmatrix} \Gamma & -\frac{v_{th}^2}{\rho^{(0)}R}\delta_{k1} & 0 & 0 & 0 \\ \left(\frac{2\rho^{(0)}}{R}-\frac{\rho_c^{(1)}}{r}\right)\frac{\Delta\theta}{\sin\Delta\theta}\delta_{k1} & \Gamma & -\frac{v_\theta^{(1)}}{r} & 0 & -\frac{f\rho^{(0)}}{r} \\ \frac{\rho_s^{(1)}}{r}\frac{\Delta\theta}{\sin\Delta\theta}\delta_{k1} & \frac{v_\theta^{(1)}}{r} & \Gamma & \frac{f\rho^{(0)}}{r} & 0 \\ -\frac{v_{bc}^{(1)}}{r}\frac{\Delta\theta}{\sin\Delta\theta}\delta_{k1} & 0 & -\frac{fv_{th}^2}{\rho^{(0)}r} & \Gamma & -\frac{v_\theta^{(1)}}{r} \\ \frac{v_{bs}^{(1)}}{r}\frac{\Delta\theta}{\sin\Delta\theta}\delta_{k1} & \frac{fv_{th}^2}{\rho^{(0)}r} & 0 & \frac{v_\theta^{(1)}}{r} & \Gamma \end{bmatrix} \cdot \begin{bmatrix} \tilde{u}_0 \\ \tilde{\rho}_{sk} \\ \tilde{\rho}_{ck} \\ \tilde{v}_{sk} \\ \tilde{v}_{ck} \end{bmatrix}$$

$$= 0, \tag{17}$$

where

$$\Gamma \equiv \frac{(\xi^2-1)\,\Delta\theta}{2\xi\,\Delta t\sin k\,\Delta\theta} \tag{18}$$

and $\delta_{k1}$ is the usual Kronecker delta. Modes with $k \geqslant 2$ decouple from those with $k = 0$, 1 and from each other. As in the analytic work it is convenient to discuss the two cases separately.

Looking only at the $k = 0$, 1 modes, we recover in the limit $\Delta\theta \to 0$ (with constant $\Delta t$) the analytical dispersion relation for small amplitude waves [6], with $i\Gamma$ taking the place of the (complex) frequency $\omega$ of the real physical mode. Therefore stability conditions on $\Delta t$ and $\Delta\theta$ can be obtained by expressing the amplification factor in terms of the actual physical frequency. From Eq. (18) then,

$$\xi^2 + (i\omega/\alpha)\,\xi - 1 = 0, \tag{19}$$

with

$$\alpha \equiv \Delta\theta/2\Delta t\sin\Delta\theta.$$

Hence

$$\xi = -(i\omega/2\alpha) \pm (1-\omega^2/4\alpha^2)^{1/2}. \tag{20}$$

If $\omega_I < \alpha$ (i.e. the Courant–Friedrichs–Lewy condition [16], $\omega_I\,\Delta t/\Delta\theta < 1$) we have

$$\xi \approx \pm 1 + \frac{(\omega_I - i\omega_R)}{2\alpha} \mp \frac{\omega_R{}^2 - \omega_I{}^2 + 2i\omega_R\omega_I}{2\alpha^2} + \cdots. \tag{21}$$

Thus each physical mode gives rise to two numerical modes, one of which behaves correctly. If $\omega_I \neq 0$ the other may soon completely dominate the calculation. This is the classic example of a "weak" instability—Morton [17, 18] has called this the interlaced mesh instability. For a purely growing mode the parasitic solution will decay in a time comparable to the rise time of the real physical instability and little

harm will be encountered. On the other hand, the physically damped modes will not be simulated correctly by this scheme, and the mesh instability will cause violent fluctuations between the two grids if allowed to persist.

In our physical model both damped and growing modes are present (in fact it is the transfer of energy between these modes which provides for the instability), and these may be propagating or stationary. In general, then, the extra numerical modes cannot be tolerated and must be filtered out before they have grown too large. The growth rates of these unwanted modes are comparable with the period of oscillation, and our experience has been that to operate anywhere near the maximum ratio of $\Delta t/\Delta\theta$ allowed by the Courant–Friedrichs–Lewy condition (applied to the acoustic oscillations), the unwanted mode must be destroyed every few time steps. Simple averaging across the two grids provides the easiest way to do this, but increases the truncation error—this is unacceptable if done too often. Earlier programs [10, 12] did not suffer from these modes because their algorithms provided tighter coupling of the two grids. It is interesting to note that a scheme using the auxiliary equations (12) to (14) with $\sigma = \sqrt{5} - 2$, $\kappa = \sqrt{5} - 1$ for both grids, does not suffer from this difficulty since the unwanted mode always decays; unfortunately the scheme is only first order accurate in $\Delta\theta$.

Turning to the modes with $k > 1$, we note that no matter how small we make $\Delta\theta$, we can always find a $k$ such that $\sin k\,\Delta\theta/\Delta\theta$ is large. Thus $\alpha$ can be small for any choice of $\Delta t$ and instability can occur. Fortunately, in the model the damping of the physical modes is very slow (on the diffusion time scale $\sim\epsilon^3$ whereas the

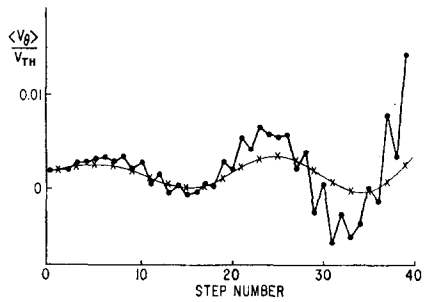


FIG. 3. Plot of average rotation velocity as a function of time for a toroidal system with $n_{max} = 10^{13}\,cm^{-3}$, $T = 25$ eV, $B = 10^4$ G, $a = 5$ cm, $R = 100$ cm, $f = 1/30$, and classical resistivity. On the plotted surface, $r = 4.62$ cm, $n = 4 \cdot 10^{12}\,cm^{-3}$, $n' = -8 \cdot 10^{11}\,cm^{-4}$, so that from Ref. 6 the oscillatory modes should damp and the rotational mode should grow with $\gamma \sim 6 \cdot 10^3\,sec^{-1}$. Each mesh has six radial and eight azimuthal surfaces; $\Delta t = 4\,\mu s$. This illustrates the growth of the unwanted computational mode when employing a leapfrog scheme (dotted curve) where damped physical modes are present. The Lax–Wendroff scheme (crossed curve) gives a more faithful representation of the physics. The observed growth of oscillations may be due to the size of the time step.

$k = 1$ modes vary as $\epsilon$) so the extra numerical ones may cause little difficulty. Since they have short wavelengths there may be some dispersion and phase mixing introduced by the finite mesh. Introduction of viscosity into the momentum conservation equation provides an additional physical dissipation mechanism that strongly damps them. This was incorporated into previous programs [12]. In any event these unwanted modes provide a source of worry in applying any leapfrog scheme.

In Fig. 3 we illustrate the growth of the unwanted mode for this problem. Here we have plotted the value of $v_\theta$, averaged over a magnetic surface, as a function of time. The oscillations represent the passage of geodesic waves (acoustic waves modified by the toroidal nature of the system) [19] whose amplitude is actually damped as time proceeds. Superimposed on this oscillation is the build-up of rotation in the $\theta$-direction—the so-called rotational instability [1–6]. The wild fluctuations experienced by the leapfrog scheme soon grow to such an extent that they completely dominate the real calculation and make the density go negative.

In practice then (for our particular problem) the leapfrog scheme is only useful if we take time-steps very much shorter than the smallest period of oscillation of any mode present. To follow the growth of unstable modes this is too restrictive, and in the next section we see how the Lax–Wendroff scheme improves the situation.

## 5. The Lax–Wendroff Scheme

By repeating the procedure described above we obtain a numerical dispersion relation similar to Eq. (16), but with

$$D_{11} = \frac{(\lambda - 1)}{2\Delta t} + \frac{\Delta t\, v_{th}^2}{\rho^{(0)} R}\left(\frac{2\rho^{(0)}}{R} - \frac{\rho_c^{(1)}}{r}\right)\left(\frac{\sin \Delta\theta}{\Delta\theta}\right)^2 \delta_{k1},$$

$$D_{12} = -\frac{v_{th}^2}{\rho^{(0)} R}\frac{\sin 2\Delta\theta}{2\Delta\theta}\,\delta_{k1},$$

$$D_{13} = -\frac{\Delta t\, v_{th}^2 v_\theta^{(1)}}{\rho^{(0)} R r}\left(\frac{\sin \Delta\theta}{\Delta\theta}\right)^2 \delta_{k1},$$

$$D_{14} = 0,$$

$$D_{15} = -\frac{\Delta t f v_{th}^2}{Rr}\left(\frac{\sin \Delta\theta}{\Delta\theta}\right)^2 \delta_{k1},$$

$$D_{21} = \left(\frac{2\rho^{(0)}}{R} - \frac{\rho_c^{(1)}}{r}\right)\frac{\sin \Delta\theta}{\Delta\theta}\,\delta_{k1} + \frac{\Delta t(f\rho^{(0)} v_{vs}^{(1)} + v_\theta^{(1)} \rho_s^{(1)})}{r^2}\left(\frac{\sin \Delta\theta}{\Delta\theta}\right)^2 \delta_{k1},$$

$$D_{22} = \frac{(\lambda - 1)}{2\Delta t} + \frac{\Delta t(v_\theta^{(1)2} + f^2 v_{th}^2)}{r^2}\left(\frac{\sin k\,\Delta\theta}{\Delta\theta}\right)^2 + \frac{\Delta t\, v_{th}^2}{\rho^{(0)} R}\left(\frac{2\rho^{(0)}}{R} - \frac{\rho_c^{(1)}}{r}\right)\left(\frac{\sin \Delta\theta}{\Delta\theta}\right)^2 \delta_{k1},$$

$$D_{23} = -\frac{v_\theta^{(1)}}{r}\frac{\sin 2k\,\Delta\theta}{2\Delta\theta},$$

$$D_{24} = \frac{2\Delta t f\rho^{(0)} v_\theta^{(1)}}{r^2}\frac{\sin k\,\Delta\theta}{\Delta\theta},$$

$$D_{25} = -\frac{f\rho^{(0)}}{r}\frac{\sin 2k\,\Delta\theta}{2\Delta\theta},$$

$$D_{31} = \frac{\rho_s^{(1)}}{r}\frac{\sin \Delta\theta}{\Delta\theta}\delta_{k1} + \frac{\Delta t}{r}\left[\frac{f\rho^{(0)} v_{bc}^{(1)}}{r} - v_\theta^{(1)}\left(\frac{2\rho^{(0)}}{R} - \frac{\rho_c^{(1)}}{r}\right)\right]\left(\frac{\sin \Delta\theta}{\Delta\theta}\right)^2 \delta_{k1},$$

$$D_{32} = \frac{v_\theta^{(1)}}{r}\frac{\sin 2k\,\Delta\theta}{2\Delta\theta} + \frac{\Delta t\, v_{th}^2 \rho_s^{(1)}}{\rho^{(0)} Rr}\left(\frac{\sin \Delta\theta}{\Delta\theta}\right)^2 \delta_{k1},$$

$$D_{33} = \frac{(\lambda - 1)}{2\Delta t} + \frac{\Delta t(v_\theta^{(1)2} + f^2 v_{th}^2)}{r^2}\left(\frac{\sin k\,\Delta\theta}{\Delta\theta}\right)^2,$$

$$D_{34} = \frac{f\rho^{(0)}}{r}\frac{\sin 2k\,\Delta\theta}{2\Delta\theta},$$

$$D_{35} = \frac{2\Delta t f\rho^{(0)} v_\theta^{(1)}}{r^2}\left(\frac{\sin k\,\Delta\theta}{\Delta\theta}\right)^2,$$

$$D_{41} = -\frac{v_{bc}^{(1)}}{r}\frac{\sin \Delta\theta}{\Delta\theta}\delta_{k1} + \frac{\Delta t}{\rho^{(0)} r^2}(\rho^{(0)} v_\theta^{(1)} v_{bc}^{(1)} + f v_{th}^2 \rho_s^{(1)})\left(\frac{\sin \Delta\theta}{\Delta\theta}\right)^2 \delta_{k1},$$

$$D_{42} = \frac{2\Delta t f v_\theta^{(1)} v_{th}^2}{\rho^{(0)} r^2}\left(\frac{\sin k\,\Delta\theta}{\Delta\theta}\right)^2 - \frac{\Delta t\, v_{th}^2 v_{bc}^{(1)}}{\rho^{(0)} Rr}\left(\frac{\sin \Delta\theta}{\Delta\theta}\right)^2 \delta_{k1},$$

$$D_{43} = -\frac{f v_{th}^2}{\rho^{(0)} r}\frac{\sin 2k\,\Delta\theta}{2\Delta\theta},$$

$$D_{44} = \frac{(\lambda - 1)}{2\Delta t} + \frac{\Delta t(v_\theta^{(1)2} + f^2 v_{th}^2)}{r^2}\left(\frac{\sin k\,\Delta\theta}{\Delta\theta}\right)^2,$$

$$D_{45} = -\frac{v_\theta^{(1)}}{r}\frac{\sin 2k\,\Delta\theta}{2\Delta\theta},$$

$$D_{51} = \frac{v_{bs}^{(1)}}{r}\frac{\sin \Delta\theta}{\Delta\theta}\delta_{k1} + \frac{\Delta t}{\rho^{(0)}r}\left[\rho^{(0)}v_\theta^{(1)}v_{bc}^{(1)} - fv_{th}^2\left(\frac{2\rho^{(0)}}{R} - \frac{\rho_c^{(1)}}{r}\right)\right]\left(\frac{\sin \Delta\theta}{\Delta\theta}\right)^2\delta_{k1},$$

$$D_{52} = \frac{fv_{th}^2}{\rho^{(0)}r}\frac{\sin 2k\,\Delta\theta}{2\Delta\theta} + \frac{\Delta t\, v_{th}^2 v_{bs}^{(1)}}{\rho^{(0)}Rr}\left(\frac{\sin \Delta\theta}{\Delta\theta}\right)^2\delta_{k1},$$

$$D_{53} = \frac{2\Delta t f v_{th}^2 v_\theta^{(1)}}{\rho^{(0)}r^2}\left(\frac{\sin k\,\Delta\theta}{\Delta\theta}\right)^2,$$

$$D_{54} = \frac{v_\theta^{(1)}}{r}\frac{\sin 2k\,\Delta\theta}{2\Delta\theta},$$

$$D_{55} = \frac{(\lambda - 1)}{2\Delta t} + \frac{\Delta t(v_\theta^{(1)2} + f^2 v_{th}^2)}{r^2}\left(\frac{\sin k\,\Delta\theta}{\Delta\theta}\right)^2. \tag{22}$$

Again the $k = 0, 1$ modes couple to give a $5 \times 5$ system, while the modes for $k \geqslant 2$ separate and yield a fourth-order one and it is convenient to discuss the two sets separately.

(i) $k = 0, 1$

Examination of the elements of **D** shows that as $\Delta t, \Delta\theta \to 0$ each element behaves asymptotically as

$$D_{ij} \sim D_{ij}^{\text{phys}} + O(\Delta t, \Delta\theta^2). \tag{23}$$

Thus (in the limit) the numerical dispersion relation behaves exactly as the analogous analytical dispersion relation [6] $D_{ij}^{\text{phys}}$, and we may make the identification

$$i\omega \to (\lambda - 1)/2\,\Delta t. \qquad (\Delta t, \Delta\theta \to 0). \tag{24}$$

Employing a perturbation expansion for the roots, we can easily establish the validity of an asymptotic expansion for the amplification factor of the form

$$(\lambda - 1)/2\,\Delta t = i\omega + \alpha_1\,\Delta t + \alpha_2\,\Delta t^2 + \beta_1\,\Delta\theta^2 + \beta_2\,\Delta\theta^3 + \cdots. \tag{25}$$

Convergence follows for the lowest frequency modes. In the absence of higher $k$ modes Eq. (25) provides "practical" stability conditions in the sense that the coefficients $\alpha_i$, $\beta_i$ (which can be easily evaluated, at least numerically, given the eigen-values and eigen-vectors of $D_{ij}^{\text{phys}}$) determine the departure of the numerical solution from the real physical situation.

(ii) $k \geqslant 2$

To establish the convergence of the scheme we must show that there are no modes present which experience a growth rate which does not asymptotically

approach the correct physical value. From Eq. (22) we see that the arguments given above cannot be carried over when $k \geqslant 2$; there will always exist some $k$ for which $k\,\Delta\theta \approx n\pi/2$ (with $n$ integral) so that (25) becomes

$$(\lambda - 1)/2\,\Delta t = i\omega + \eta_1(\Delta t/\Delta\theta^2) + \eta_2(\Delta t/\Delta\theta^2)^2 + \alpha_1\,\Delta t + \beta_1\,\Delta\theta^2 + \cdots. \quad (26)$$

Clearly this shows convergence in the limit $\Delta t, \Delta\theta \to 0$ provided $\Delta t/\Delta\theta^2 \to 0$, but the practical stability criterion $\Delta t \ll \Delta\theta^2$, usually associated with parabolic rather than hyperbolic systems, is very restrictive.

In fact we can demonstrate stability in much less stringent conditions [20] by rewriting the system of equations (9)–(14), for $k \geqslant 2$ as

$$\tilde{\mathbf{y}}^{2n+1} = \tilde{\mathbf{y}}^{2n-1} - \alpha\mathbf{A} \cdot \delta\tilde{\mathbf{y}}^{2n}, \quad (27)$$

$$\tilde{\mathbf{y}}^{2n} = \mu(\tilde{\mathbf{y}}^{2n-1}) - \tfrac{1}{2}\alpha\mathbf{A} \cdot \delta\tilde{\mathbf{y}}^{2n-1}, \quad (28)$$

where

$$\tilde{\mathbf{y}}^{2n} \equiv \begin{pmatrix} \rho\tilde{v}^{2n+1} \\ v_{th}\tilde{\rho}^{2n+1} \end{pmatrix},$$

$$\alpha \equiv \frac{\Delta t}{\Delta\theta},$$

and

$$\mathbf{A} \equiv \frac{1}{r^2}\begin{pmatrix} v_\theta & fv_{th} \\ fv_{th} & v_\theta \end{pmatrix}.$$

The amplification matrix for this system, Eq. (27) and (28), is

$$\mathbf{G} = \mathbf{I} + 2i\mathbf{W} \cdot (i\mathbf{W} - \cos k\,\Delta\theta\,\mathbf{I}), \quad (29)$$

where $\mathbf{W} \equiv \alpha\mathbf{A} \sin k\,\Delta\theta$. Now for any vector solution $\mathbf{y}$ we can easily show that

$$|\,\mathbf{y}^* \cdot \mathbf{G} \cdot \mathbf{y}\,|^2 = (\|\,\mathbf{y}\,\|^2 - 2\,\|\,\mathbf{W} \cdot \mathbf{y}\,\|^2)^2 + 4\cos^2 k\,\Delta\theta\,|\,\mathbf{y}^* \cdot \mathbf{W} \cdot \mathbf{y}\,|^2$$

$$\leqslant \|\,\mathbf{y}\,\|^4 \left\{1 - \frac{4\,\|\,\mathbf{W} \cdot \mathbf{y}\,\|^2}{\|\,\mathbf{y}\,\|^2}\left[1 - \frac{\|\,\mathbf{W} \cdot \mathbf{y}\,\|^2}{\|\,\mathbf{y}\,\|^2} - \cos^2 k\,\Delta\theta\right]\right\}$$

($\|\,\mathbf{y}\,\|$ is the norm of $\mathbf{y}$). Since $\|\,\mathbf{W} \cdot \mathbf{y}\,\| \leqslant \|\,\mathbf{W}\,\|\,\|\,\mathbf{y}\,\|$, we see that the Lax–Wendroff condition for stability [16] is satisfied provided

$$\|\,\mathbf{A}\,\|\,\Delta t/\Delta\theta \leqslant 1,$$

the Courant–Friedrichs–Lewy condition (as may have been expected). Thus we have the stability condition

$$\left[\frac{|v_\theta| + fv_{th}}{r}\right]\frac{\Delta t}{\Delta\theta} \leqslant 1. \tag{30}$$

Reference to figure 3 shows that the Lax–Wendroff scheme provides a more realistic simulation of the physical conditions prevailing.

## 6. Discussion

In this work we have carried through a local stability analysis [16] of two numerical schemes, leapfrog and Lax–Wendroff, for a special hydromagnetic model for two-dimensional low pressure plasma confinement in a system with a large aspect ratio. The exciting feature is that the resulting dispersion relation which determines the amplification factor is strikingly similar to the analogous dispersion relation obtained by an analytic calculation [6].

The most essential feature of the small inverse-aspect-ratio expansion is the decoupling of the magnetic surfaces (because $v_r \sim \epsilon^2$) which reduces the stability discussion of the two-dimensional simulation to a one-dimensional problem. This separation is due to the fact that the diffusion time is long compared to the time scales of particular interest. Since this should be the case for an operating thermonuclear reactor, the physics makes our conclusions concerning the applicability of the code a little more reasonable than the analysis would indicate. It would be interesting to attempt a stability analysis of the two-dimensional code without assuming small resistivity. The difficulty lies primarily in the fact that one would have no idea what answer to expect from the physics.

The small inverse-aspect-ratio expansion also separates the $k \geqslant 2$ modes from those with $k = 0$, 1 and from each other. Thus, relating $\lambda$ and $\omega$ by Eq. (24) and taking $\Delta t$ and $\Delta\theta$ sufficiently small makes the amplification matrix identical to the physical dispersion relation. Although this identification would probably not be exact in more general systems [14, 15] where the mode decoupling doesn't occur, it is reasonable to expect that the numerical scheme should still closely approximate the physics.

Finally, all local analyses like the one given here are subject to the limitation that we can infer nothing for cases where the "perturbation" $\tilde{\rho}$ becomes as large as the "steady-state" value $\rho$. This difficulty is common to many stability analyses. It may be more serious in the specific applications being made of these codes than in other cases because "shocks" or regions where large density variations exist can develop in the system [7, 9]. By properly choosing new functions for the $\rho$'s

it is possible that conditions for stability of the code even in these extreme cases can be studied. In the absence of such work it is comforting to know that the analytically predicted shock solutions have been observed in the simulations [12].

To summarize then, we have adopted a simple small-inverse-aspect ratio model and shown that provided the Courant–Friedrichs–Lewy condition [16] is satisfied, a simple Lax–Wendroff scheme possesses local stability in the sense that perturbations from what would be predicted by the analytic equations should not grow. The amplification matrix for the simulation is closely related to the analogous dispersion relation obtained from the analytic treatment such that it is reasonable to assume that the numerical algorithm should be good for more general physical models.

## ACKNOWLEDGMENTS

We are deeply indebted to K. W. Morton for many helpful discussions, suggestions and much guidance. One of us (J. L. J.) is indebted to R. S. Pease and J. B. Taylor for their hospitality during his stay at Culham when some of this work was done and to M. B. Gottlieb for making the visit possible. He was supported by USAEC Contract AT(11-1)-3073 with Princeton University.

## REFERENCES

1. T. E. STRINGER, *Phys. Rev. Lett.* **22** (1969), 770.
2. M. N. ROSENBLUTH AND J. B. TAYLOR, *Phys. Rev. Lett.* **23** (1969), 367.
3. A. A. GALEEV, *Zh.E.T.F. Pis. Red.* **10** (1969), 353. [*J.E.T.P. Lett.* **10** (1970), 225].
4. H. P. ZEHRFELD AND B. J. GREEN, *Nucl. Fus.* **10** (1970), 251.
5. O. P. POGUTSE, *Nucl. Fus.* **10** (1970), 399.
6. J. M. GREENE, J. L. JOHNSON, K. E. WEIMER AND N. K. WINSOR, *Phys. Fluids* **14** (1971), 1258.
7. E. C. BOWERS AND N. K. WINSOR, *Phys. Fluids* **14** (1971), 2203.
8. R. C. GRIMM AND J. L. JOHNSON, *Plasma Physics* **14** (1972), 617.
9. J. M. GREENE AND N. K. WINSOR, *Phys. Fluids* (in press).
10. N. K. WINSOR, J. L. JOHNSON AND J. M. DAWSON, *J. Comp. Phys.* **6** (1970), 430.
11. M. G. HAINES, *Phys. Rev. Lett.* **25** (1970), 1480.
12. E. C. BOWERS AND N. K. WINSOR, Proceedings of the 4th. Conf. on Numerical Simulation of Plasmas, Navy Research Laboratories, Washington (1970).
13. M. A. HELLBERG, N. K. WINSOR, J. M. DAWSON AND J. L. JOHNSON, *Bull. Am. Phys. Soc. II*, **16** (1971), 1240.
14. R. C. GRIMM, J. L. JOHNSON AND N. K. WINSOR, to be published.
15. R. C. GRIMM AND J. L. JOHNSON, to be published.
16. R. D. RICHTMEYER AND K. W. MORTON, "Difference Methods for Initial-Value Problems," Interscience, New York (1967).
17. K. W. MORTON, *in* Proceedings of the Computational Physics Conference, UKAEA Culham Laboratory and The Institute of Physics and The Physical Society (1969), Vol. 1, Paper F
18. K. W. MORTON, *Proc. Roy. Soc.* **A323** (1971), 237.
19. N. K. WINSOR, J. L. JOHNSON AND J. M. DAWSON, *Phys. Fluids* **11** (1968), 2448.
20. K. W. MORTON, private communication.